Application of linear and nonlinear fracture mechanics options to free edge delamination in laminated composites

J. C. J. SCHELLEKENS and R. DE BORST
Delft University of Technology
Department of Civil Engineering
TNO Building and Construction Research
The Netherlands

Abstract

Free edge delamination of a graphite-epoxy specimen is simulated using nonlinear finite element analysis, linear elastic fracture mechanics and a "reduced stiffness method" based on classical laminated plate theory. The theoretical background of the three different approaches is discussed. For use in the nonlinear finite element approach generalised plane strain elements and 3D line interface elements have been developed. By analysing delamination in $[+25_n/-25_n/90_n]_s$ laminates, the predictive value of the different methods is investigated.

KEYWORDS: Delamination; Edge Effects; Failure Mechanism;
Nonlinear Finite Element Analysis; Mode-I; Fracture Mechanics

1 Introduction

A failure mode often encountered in structural composite laminates is delamination, a phenomenon which has great influence on structural integrity. In the last two decades much research has concentrated on the complex mechanism of delamination. Due to the anisotropic material properties and the varying fibre orientations each ply in the laminate behaves differently. Consequently, edge stresses are then necessary to preserve compatibility of the deformations. These large transverse normal and shear stresses are primarily responsible for initiating delamination. Analytical models have been developed for the treatment of free edge stress distributions in [1, 2, 3]. A historical review of these models is given by Pagano and Soni [4]. Furthermore procedures to predict delamination onset and growth based on the principle of virtual crack extension have been applied by Crossman, Wang [5, 6] and O'Brien [7] amongst others. Because of the stress singularities that exist at the ply interfaces near the free edges and the resulting mesh-dependency it is commonly believed that the use of stress-based failure criteria does not produce relevant results as far as free edge delamination is concerned. However, Kim and Soni [8] indicated that an average stress approach combined with an anisotropic failure criterion results in an accurate prediction of the onset of delamination. The essential feature of their approach is the introduction of the ply thickness in the determination of stresses.

In this contribution a nonlinear finite element procedure is developed for the prediction of delamination onset and growth. Although the failure criterion is based on stresses it is shown that, when combined with a softening type of post-crack response, a stress-based failure criterion results in a mesh-objective calculation. The performance of the method is demonstrated via the analyses of free edge delamination in $[+25_n/-25_n/90_n]_s$ graphite-epoxy specimens under uniaxial tension.
In the examples twelve-noded cubic generalised plane strain elements have been used with three translational degrees-of-freedom in each node. These elements, which are assumed to remain elastic during the loading process, give an accurate representation of the stress concentrations near the free edges without the need for extreme mesh refinement. The individual plies are connected by cubic 3D line interface elements [9, 10]. These are well suited for modelling the geometric discontinuity which arises during delamination and which can either be gradual (softening type behaviour) or perfectly brittle. In the nonlinear analyses emphasis is focused on the effects of mesh refinement and laminate thickness on the ultimate load capacity of the laminates. Furthermore the influence of the transverse tensile strength of the ply interfaces on the limit load is investigated. The results from nonlinear analyses are compared with results obtained from a virtual crack extension analysis and a reduced stiffness method.

2 Generalised plane-strain elements

In free edge delamination testing specimens are subjected to a uniaxial load. It is assumed that at a certain distance from the ends of the specimen the in-plane displacements are independent of the x-coordinate (see Fig. 1).
For the displacement field of a cross-section [1, 3, 7], this allows us to introduce:

$$\begin{aligned} u_x(x,y,z) &= \varepsilon_x x + u_x(y,z) \\ u_y(x,y,z) &= u_y(y,z) \\ u_z(x,y,z) &= u_z(y,z) \end{aligned} \tag{1}$$

with ε_x being the strain that is prescribed in the x-direction of the specimen. If we define a matrix $\boldsymbol{H}$ which contains the interpolation polynomials, so that $\boldsymbol{u} = \boldsymbol{Ha}$, and a differential operator $\boldsymbol{L}$

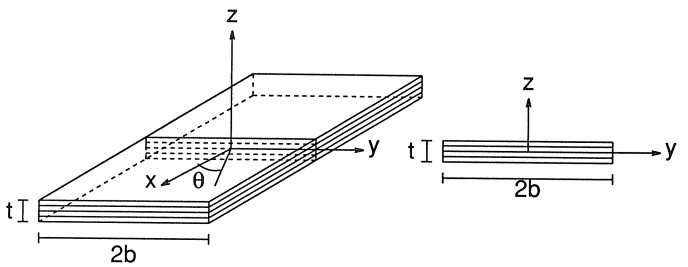

Fig. 1. Geometry of the specimen.

$$\boldsymbol{L}^{\mathrm{T}} = \begin{bmatrix} 0 & 0 & 0 & 0 & \frac{\partial}{\partial z} & \frac{\partial}{\partial y} \\ 0 & \frac{\partial}{\partial y} & 0 & \frac{\partial}{\partial z} & 0 & 0 \\ 0 & 0 & \frac{\partial}{\partial z} & \frac{\partial}{\partial y} & 0 & 0 \end{bmatrix} \tag{2}$$

we obtain

$$\boldsymbol{\varepsilon} = \boldsymbol{B}\boldsymbol{a} + \boldsymbol{\varepsilon}_1 \tag{3}$$

where $\boldsymbol{\varepsilon}_1 = (\varepsilon_x, 0, 0, 0, 0, 0)$ denotes the externally applied strain vector and $\boldsymbol{B} = \boldsymbol{L}\boldsymbol{H}$ is the strain displacement matrix.

In a nonlinear analysis the total load is applied in an incremental fashion. Within each loading step equilibrium is achieved in an iterative manner, which is different from linear elastic analyses. For the incremental strains $\delta\boldsymbol{\varepsilon}_j$ in a nonlinear analysis we can write

$$\delta\boldsymbol{\varepsilon}_j = \boldsymbol{B}\delta\boldsymbol{a}_j + \delta\lambda_j\boldsymbol{\varepsilon}_1 \tag{5}$$

where j denotes the iteration number and $\delta\lambda_j = \Delta\lambda_j - \Delta\lambda_{j-1}$ is the change in value of the incremental load parameter λ from iteration $j-1$ to iteration j. The incremental nodal displacement vector is given by $\delta\boldsymbol{a}_j$. From eq. (5) it follows with $\boldsymbol{D}$ the elastic stress-strain matrix for the plies, that the incremental stresses are given by

$$\delta\boldsymbol{\sigma}_j = \boldsymbol{D}(\boldsymbol{B}\delta\boldsymbol{a}_j + \delta\lambda_j\boldsymbol{\varepsilon}_1) \tag{6}$$

If $\boldsymbol{\sigma}_{j-1}$ represents the total stress vector at the end of iteration $j-1$, then the total stress at the end of iteration j reads

$$\boldsymbol{\sigma}_j = \boldsymbol{\sigma}_{j-1} + \boldsymbol{D}(\boldsymbol{B}\delta a_j + \delta\lambda_j\boldsymbol{\varepsilon}_1) \tag{7}$$

The expressions for the internal and external force vectors for strain loading then read

$$\boldsymbol{f}_j = \int_V \boldsymbol{B}^{\mathrm{T}}(\boldsymbol{\sigma}_j - \lambda_j\boldsymbol{D}\boldsymbol{\varepsilon}_1)\,\mathrm{d}V \quad \text{and} \quad \boldsymbol{f}_e = -\lambda_0 \int_V \boldsymbol{B}^{\mathrm{T}}\boldsymbol{D}\boldsymbol{\varepsilon}_1\,\mathrm{d}V \tag{8}$$

where λ_0 is the total load factor at the beginning of the current step. If the structural stiffness matrix is denoted by $\boldsymbol{K}$ the incremental displacements can be solved iteratively from

$$\boldsymbol{K}\delta\boldsymbol{a}_j = \boldsymbol{f}_e - \boldsymbol{f}_{j-1}. \tag{9}$$

3 Indirect displacement control for strain loading

A major drawback of load-controlled calculations is the fact that no limit points can be passed. Riks [11] developed an "arc-length" method to overcome this limitation. In this method the incremental load factor is constrained by the norm of the incremental

displacement vector. Although the arc-length control method has proved to be fairly successful, it has been reported to fail in situations of highly localised failure. It was suggested by De Borst [12] that the displacement norm should in these cases be determined by considering only the dominant degrees of freedom. In conventional strain loading the incremental nodal displacements are determined from eq. (8) in an iterative manner. In an arc-length modification of strain loading this process can be represented by the following set of equations [12] (for iteration j)

$$\delta \boldsymbol{a}_j^{\mathrm{I}} = -\boldsymbol{K}_{j-1}^{-1}(\lambda_0 \int_V \boldsymbol{B}^{\mathrm{T}} \boldsymbol{D} \boldsymbol{\varepsilon}_1 \, \mathrm{d}V + \int_V \boldsymbol{B}^{\mathrm{T}}(\boldsymbol{\sigma}_{j-1} - \lambda_{j-1} \boldsymbol{D} \boldsymbol{\varepsilon}_1) \, \mathrm{d}V) \tag{10}$$

$$\delta \boldsymbol{a}_j^{\mathrm{II}} = -\boldsymbol{K}_{j-1}^{-1} \int_V \boldsymbol{B}^{\mathrm{T}} \boldsymbol{D} \boldsymbol{\varepsilon}_1 \, \mathrm{d}V \tag{11}$$

$$\delta \boldsymbol{a}_j = \delta \boldsymbol{a}_j^{\mathrm{I}} + \delta \lambda_j \delta \boldsymbol{a}_j^{\mathrm{II}} \tag{12}$$

$$\Delta \boldsymbol{a}_j = \Delta \boldsymbol{a}_{j-1} + \delta \boldsymbol{a}_j \tag{13}$$

where $\Delta \boldsymbol{a}_j$ denotes the total incremental displacement vector. It is determined on the basis of the requirement that the Crack Opening Displacement (COD) of the interface between two plys where delamination occurs should have a constant value for each iteration,

$$\delta(\mathrm{COD}) = 0 \Rightarrow \delta a_j^n - \delta a_j^m = 0$$

where δa_j^n is the change in displacement in the thickness direction of the laminate of node n from iteration $j-1$ to j.

4 Formulation of interface elements and discrete cracking

The individual plies in the laminate are connected by interface elements (see Fig. 2). These elements have the ability to model the geometrical discontinuity that is introduced by delamination. In the elastic stage of the calculation no additional deformations are allowed in the finite element model because of these interface elements. Therefore a sufficiently high dummy stiffness has to be supplied. Unlike continuum elements, interface elements do not keep track of stresses and strains at the integration

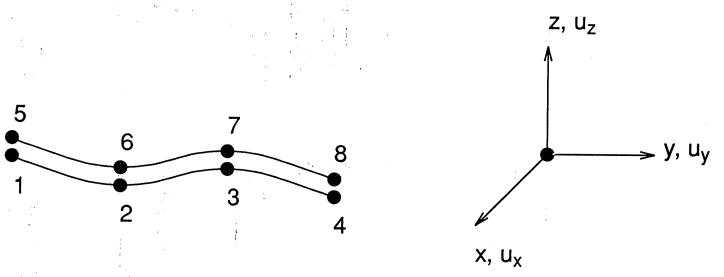

Fig. 2. Cubic line interface element with nodal degrees of freedom.

points, but consider tractions and relative displacements. With the differential operator matrix $\boldsymbol{L}$ and the interpolation matrix $\boldsymbol{H}$ defined as

$$\boldsymbol{L}=\begin{bmatrix} -1 & +1 & 0 & 0 & 0 & 0 \\ 0 & 0 & -1 & +1 & 0 & 0 \\ 0 & 0 & 0 & 0 & -1 & +1 \end{bmatrix} \qquad \boldsymbol{H}=\begin{bmatrix} \boldsymbol{n} & 0 & 0 & 0 & 0 & 0 \\ 0 & \boldsymbol{n} & 0 & 0 & 0 & 0 \\ 0 & 0 & \boldsymbol{n} & 0 & 0 & 0 \\ 0 & 0 & 0 & \boldsymbol{n} & 0 & 0 \\ 0 & 0 & 0 & 0 & \boldsymbol{n} & 0 \\ 0 & 0 & 0 & 0 & 0 & \boldsymbol{n} \end{bmatrix} \tag{14}$$

with $\boldsymbol{n}$ representing the interpolation polynomial vector and the nodal displacement vector

$$\boldsymbol{a}=(u_{\mathrm{z}}^{1}, u_{\mathrm{z}}^{2}, \ldots, u_{\mathrm{z}}^{\mathrm{n}}, u_{\mathrm{y}}^{1}, u_{\mathrm{y}}^{2}, \ldots, u_{\mathrm{y}}^{\mathrm{n}}, u_{\mathrm{x}}^{1}, u_{\mathrm{x}}^{2}, \ldots, u_{\mathrm{x}}^{\mathrm{n}}), \tag{15}$$

the relative displacements are related to the nodal displacements through

$$\Delta\boldsymbol{u}=\boldsymbol{LHa}. \tag{16}$$

If we use $\boldsymbol{D}$ to denote the tangent stiffness matrix, the tractions $\boldsymbol{t}=(t_{\mathrm{z}}, t_{\mathrm{y}}, t_{\mathrm{x}})$ are obtained from

$$\boldsymbol{t}=\boldsymbol{D}\Delta\boldsymbol{u}. \tag{17}$$

For a line interface element in a generalised plane strain situation the element stiffness matrix is derived as

$$\boldsymbol{K}=\int_{\xi=-1}^{\xi=+1} \boldsymbol{B}^{\mathrm{T}}\boldsymbol{D}\boldsymbol{B}\frac{\partial x}{\partial \xi}\,\mathrm{d}\xi. \tag{18}$$

Once the elastic limit in an integration point of the interface element is exceeded, the traction-relative displacement relation $\boldsymbol{D}$ becomes nonlinear and is determined by a discrete crack model. In the present model crack initiation is supposed to be purely in mode-I. A crack arises when the traction t_{z} normal to the plies exceeds the tensile strength f_{t}. It is recognised that a stress criterion cannot predict the onset of delamination correctly. Depending on the type of material the traction and stiffness in a mode-I crack may abruptly or gradually reduce to zero. The first phenomenon is called brittle failure, whereas the gradual decrease of crack traction and stiffness with increasing relative displacements is called softening behaviour. The use of a softening type of response results in a rate-controlled delamination. Fig. 3 shows four different types of post-crack response; brittle failure, linear, multi-linear and nonlinear softening.

For the derivation of the nonlinear stiffness relation we will use a decomposed approach [9, 10] in which the total relative displacement consists of an elastic part $\Delta\boldsymbol{u}^{\mathrm{el}}$ and an inelastic part that is equal to the crack relative displacement $\Delta\boldsymbol{u}^{\mathrm{cr}}$. In the crack model the incremental tractions $\Delta\boldsymbol{t}$ for the intact material are given by

$$\Delta\boldsymbol{t}=\boldsymbol{D}\Delta\Delta\boldsymbol{u}^{\mathrm{el}}. \tag{19}$$

In this $\Delta\Delta\boldsymbol{u}^{\mathrm{el}}$ represents the incremental elastic relative displacement vector. The

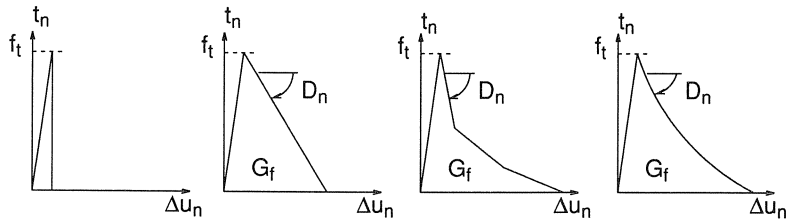

Fig. 3. Traction relative displacement relations.

incremental crack-relative displacements $\Delta\Delta \boldsymbol{u}^{\mathrm{cr}}$ are related to the incremental tractions according to

$$\Delta \boldsymbol{t} = \boldsymbol{D}^{\mathrm{cr}} \Delta\Delta \boldsymbol{u}^{\mathrm{cr}} \tag{20}$$

where $\boldsymbol{D}^{\mathrm{cr}}$ is the crack stiffness matrix which is dependent on the mode-I post crack relation. The total incremental relative displacement is written as

$$\Delta\Delta \boldsymbol{u} = \Delta\Delta \boldsymbol{u}^{\mathrm{el}} + \Delta\Delta \boldsymbol{u}^{\mathrm{cr}}. \tag{21}$$

Substituting eqs. (19) and (20) in eq. (21) results in

$$\Delta \boldsymbol{t} = [\boldsymbol{D}^{-1} + (\boldsymbol{D}^{\mathrm{cr}})^{-1}]^{-1} \Delta\Delta \boldsymbol{u}, \tag{22}$$

or using the Sherman-Morrison-Woodbury formula

$$\Delta \boldsymbol{t} = [\boldsymbol{D} - \boldsymbol{D}[\boldsymbol{D}^{\mathrm{cr}} + \boldsymbol{D}]^{-1}\boldsymbol{D}] \Delta\Delta \boldsymbol{u}. \tag{23}$$

This relation reduces to zero for brittle failure.

5 A fracture mechanics approach: virtual crack extension method

Since the early 1970s most of the research on free edge delamination has concentrated on linear elastic fracture mechanics. In this contribution we will use the approach as proposed by Wang et al. [5, 13] for the prediction of delamination onset. For the energy release rate in a free edge delamination specimen subjected to a uniaxial strain ε_{x} the following expression was introduced

$$G_{\mathrm{f}} = C_{\varepsilon} \varepsilon_{\mathrm{x}}^2 t \tag{24}$$

in which t is the ply thickness. The constant C_{ε} is determined from linear elastic fracture mechanics analyses and is equal to the value of the energy release rate in a laminate with unit ply thickness loaded by a unit strain. Having determined the value of C_{ε}, the strain at delamination onset can be calculated from eq. (24) since t and G_{f} are known. In the following the principle of virtual crack extension [14] which is applied to determine the energy release rate is discussed briefly. The potential energy π in the laminate can be written as

$$\pi = \tfrac{1}{2} \boldsymbol{a}^{\mathrm{T}} \boldsymbol{K} \boldsymbol{a} - \boldsymbol{a}^{\mathrm{T}} \boldsymbol{f}_{\mathrm{e}}. \tag{25}$$

Since the energy release rate G_f for a generalised plane strain situation equals $-(d\pi/da)$ where da denotes the crack extension we obtain after differentiation of eq. (25) with respect to a

$$G_f = -\tfrac{1}{2}\boldsymbol{a}^T \frac{\partial \boldsymbol{K}}{\partial a}\boldsymbol{a} + \boldsymbol{a}^T \frac{\partial \boldsymbol{f}_e}{\partial a}. \tag{26}$$

In this a represents the delamination length.

6 Laminated plate theory: the reduced stiffness method

Delamination in composite laminates is often accompanied by a loss of stiffness. O'Brien [7] used the correlation between the energy release rate and the extensional stiffness reduction during the delamination process to predict the onset of delamination.

For a partially delaminated specimen with a delamination length $2a$ and width $2b$ (see Fig. 4) a rule of mixtures gives the following expression for the extensional stiffness E_p

$$E_p = (E_d - E_l)\frac{a}{b} + E_l. \tag{27}$$

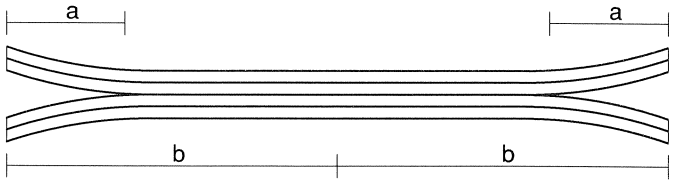

Fig. 4. Partially delaminated specimen.

E_d and E_l are the extensional stiffnesses of the completely delaminated and intact laminate respectively. If a laminate is subjected to a uniaxial strain ε_x the amount of stored energy is given by

$$\pi = \int_V \tfrac{1}{2}\varepsilon_x^2 E_p \, dV. \tag{28}$$

With volume $V = 2blt$ and delaminated surface $A = 2al$ the energy release rate G_f becomes

$$G_f = -\frac{d\pi}{dA} = -\frac{\varepsilon_x^2(E_d - E_l)t}{2} \tag{29}$$

which is independent of the delamination length a. Now, E_d and E_l have to be determined.

According to laminated plate theory [15] the extensional stiffness of the undamaged laminate equals

$$E_1 = \frac{1}{C_{11} t} \tag{30}$$

where C_{11} denotes the first component of the in-plane compliance matrix and t is the thickness of the laminate. With $\boldsymbol{A}$ the in-plane stiffness matrix that relates strains to normal forces, $\boldsymbol{B}$ a coupling matrix between bending moments and in-plane strains and $\boldsymbol{D}$ the flexural stiffness matrix that relates the bending moments to the curvatures, matrix inversion yields for the compliance matrix $\boldsymbol{C}$

$$\boldsymbol{C} = \boldsymbol{A}^{-1} + \boldsymbol{A}^{-1}\boldsymbol{B}[\boldsymbol{D} - \boldsymbol{B}\boldsymbol{A}^{-1}\boldsymbol{B}]^{-1}\boldsymbol{B}\boldsymbol{A}^{-1}. \tag{31}$$

In the case of a symmetric laminate, matrix $\boldsymbol{B}$ is a null matrix and $\boldsymbol{C}$ reduces to $\boldsymbol{A}^{-1}$. The extensional stiffness of the fully delaminated specimen is determined using a mixture rule. For each sublaminate that is formed during delamination the extensional stiffness $E_{1,i}$ is calculated using eqs. (30) and (31). If t_i denotes the thickness of the sublaminate and n is the number of sublaminates, the extensional stiffness for the completely delaminated specimen is obtained from

$$E_d = \sum_{i=1}^{i=n} \frac{E_{1,i} t_i}{t}. \tag{32}$$

If the energy release rate and the material properties for a specific laminate are known, the delamination onset strain is determined from

$$\varepsilon_c = \left(\frac{2G_f}{t(E_1 - E_d)} \right)^{1/2}. \tag{33}$$

7 Delamination in $[+25_n/-25_n/90_n]_s$ graphite epoxy laminates

For the investigation of the mesh-dependency of delamination growth a 6-ply $[\pm 25/90]_s$ graphite epoxy laminate (see Table 1 for material properties) was subjected to a uniaxial strain load [6, 13]. Since delamination is initiated at the 90/90 ply interface, the result is a pure mode-I crack extension. The dimensions of the cross-section of the laminate are 25.0 × 0.792 mm with a ply-thickness equal to 0.132 mm.

Table 1. Material properties for As-3501-06 Graphite Epoxy [N/mm^2] [13]

Young's moduli		Shear moduli		Poisson ratios	
E_{11}	$140 \cdot 10^{+3}$	G_{12}	$5.5 \cdot 10^{+3}$	ν_{12}	0.29
E_{22}	$11 \cdot 10^{+3}$	G_{13}	$5.5 \cdot 10^{+3}$	ν_{13}	0.29
E_{33}	$11 \cdot 10^{+3}$	G_{23}	$5.5 \cdot 10^{+3}$	ν_{23}	0.29

Due to the symmetry of the laminate only a quarter of the cross-section was modelled using cubic generalised plane strain elements (see Fig. 5). Translations in the z-direction along the y-axis and translations in the x- and y-directions along the z-axis were prevented.

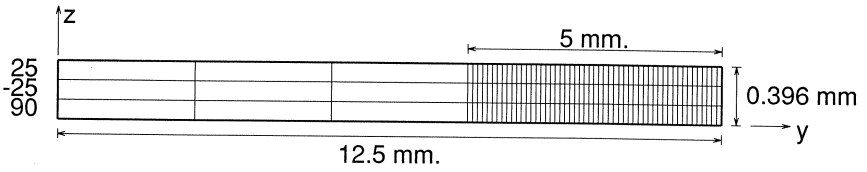

Fig. 5. Finite element mesh and dimensions.

Cubic line interface elements were supplied between the 90 degrees plies. A 4 × 4 Gauß integration scheme was used for the generalised plane strain elements. For the interface elements a nodal lumping scheme was applied since Gaußian integration leads to oscillatory traction profiles [10]. For the dummy stiffness of the interface elements a value of 10^{+8} N/mm^3 was substituted, the tensile strength was chosen equal to $f_t = 51.6$ N/mm^2 [15]. A linear softening relation is assumed to govern the post-crack response in the interface elements.

Mesh-objectivity was examined using four different meshes with a varying number of elements over the width of the specimen. In all cases the element height was equal to the ply thickness. The part of the specimen within 5 mm of the free edge was modelled using 50, 100, 200 and 400 elements respectively for each ply (element lengths: 0.1, 0.05, 0.025 and 0.0125 mm). The remaining 7.5 mm was modelled using three elements per ply. To achieve a rate-controlled delamination a fracture energy $G_f = 0.35$ N/mm was supplied. Fig. 6 shows the results for the four different meshes.

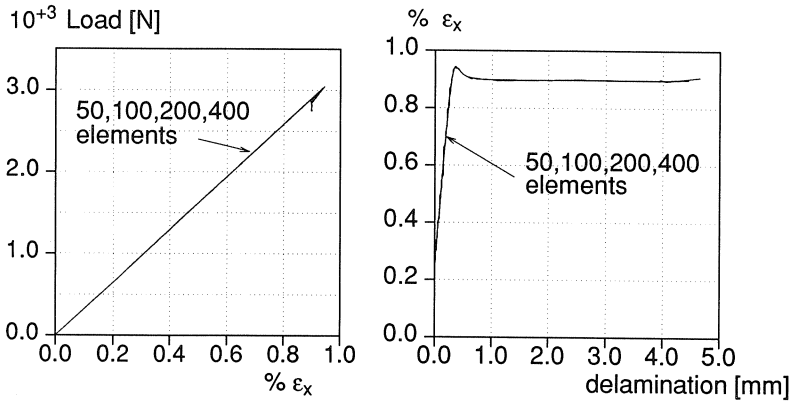

Fig. 6. Mesh-objectivity.
Left: Axial load versus applied uniaxial strain.
Right: Applied uniaxial strain versus delamination length.

It can be seen that, upon mesh refinement, the different analyses converge to the same solution. Hence, results are not influenced by the different element sizes. It should be mentioned that the snap back in the left diagram was overcome using indirect displacement control in which the crack opening displacement (COD) is used as a constraint for

the determination of the load parameter $\Delta\lambda$. Without COD-control the peak in the structural response could not be passed in a stable manner. A deformed geometry of the mesh with 100 elements per ply for a delamination of 4.37 mm is presented in Fig. 7. The scale of deformation is 1.0.

To investigate the effect of the value of the tensile strength on the ultimate tensile strain two additional analyses were performed in which f_t was varied between 90% and 110% of the original value (46.44 N/mm^2 and 56.76 N/mm^2). The results given in Fig. 8 show a maximum shift of 1.0% in the values for the ultimate uniaxial strain.

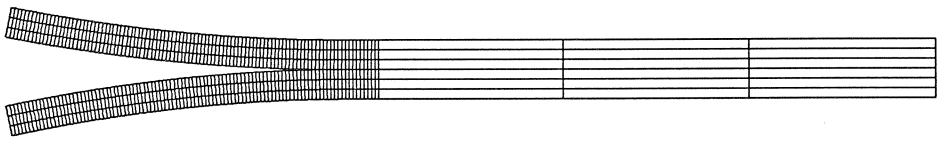

Fig. 7. Deformed laminate at a delamination length of 4.37 mm.

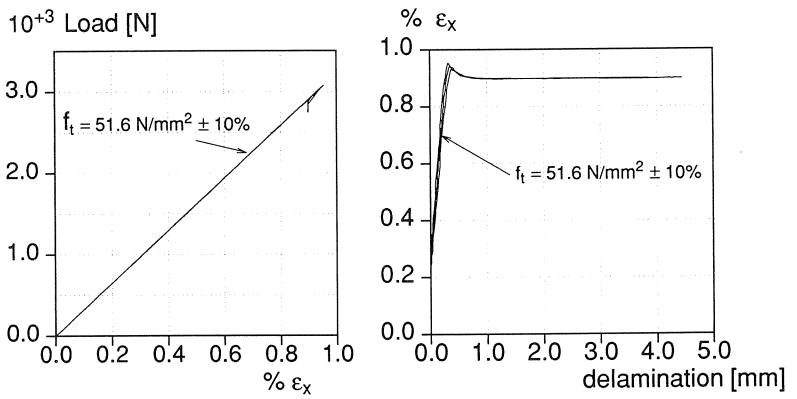

Fig. 8. Influence of 10% variation in tensile strength.
Left: Axial load versus applied uniaxial strain.
Right: Applied uniaxial strain versus delamination length.

Analyses on $[+25_n/-25_n/90_n]_s$ $(n = 1, 2, 3)$ laminates were performed to assess the capability of our approach to deal with size effects. In the analyses a fracture energy G_f equal to 0.35 N/mm and an element length of 0.05 mm were used. Fig. 9 illustrates the effect of the laminate thickness on the laminate response.

Fig. 10 compares the results obtained from nonlinear finite element analyses, the virtual crack extension method and the reduced stiffness method.

As Figs. 9 and 10 show, the ultimate strain is inversely dependent on the square root of the laminate thickness, as indicated by the dashed line. Good agreement exists between results obtained from nonlinear finite element analyses and the results from the virtual crack extension analyses. Crossman, Wang [5, 6] and O'Brien [7] reported the same dependence. Although the results from the reduced stiffness method also depend

inversely on the laminate thickness, the values do not correspond with the other results. This may cast some doubt on the merit of the reduced stiffness approach in predicting the onset of delamination. In [7] O'Brien neglected the bending effect on the stiffness reduction which resulted in an accurate prediction of mixed mode delamination. However, omission of bending effects in the case of symmetric laminates leads to an infinite value of the failure strain since the values of E_l and E_d are equal in this case.

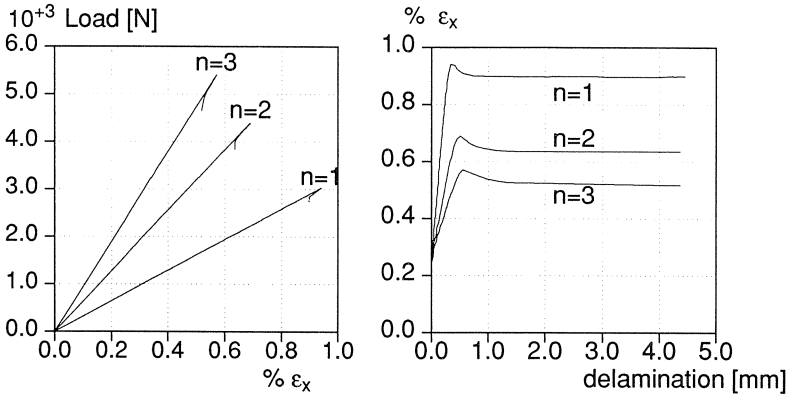

Fig. 9. Ultimate strains for $[+25_n/-25_n/90_n]_s$ $(n=1,2,3)$ laminates.
Left: Axial load versus applied uniaxial strain.
Right: Applied uniaxial strain versus delamination length.

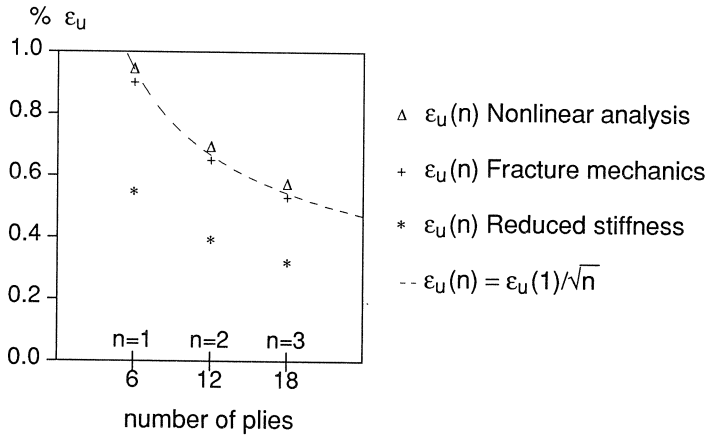

Fig. 10. Ultimate strains for $[+25_n/-25_n/90_n]_s$ $(n=1,2,3)$ laminates: A comparison between nonlinear finite element mehod, linear elastic fracture mechanics and a reduced stiffness method.

8 Concluding remarks

A nonlinear finite element approach has been proposed for the analysis of free edge delamination problems in composite laminates. Although a stress criterion is used for the initiation of delamination no influence of mesh-refinement on the ultimate

strength of the laminates is encountered. This is a result of the softening type of response that is utilised after cracking. It has been demonstrated that in the present approach the ultimate uniaxial strain is rather insensitive to changes in value of the tensile strength f_t. Furthermore it is believed that the present method results in a proper treatment of size effects. The results from nonlinear analyses are in good agreement with the results obtained from linear elastic fracture mechanics. The discrepancy that exists between the results obtained from the reduced stiffness method on one hand and the results from the nonlinear finite element method and linear elastic fracture mechanics on the other hand cast some doubt on the predictive power of this method.

References

1. Pipes R. B. and Pagano N. J., Interlaminar Stresses in Composite Laminates Under Uniform Axial Extension, Journal of Composite Materials, 4, (1970), pp. 538–544.
2. Rybicki E. F., Approximate Three-Dimensional Solutions for Symmetric Laminates Under Inplane Loading, Journal of Composite Materials, 5, (1971), pp. 354–360.
3. Pagano N. J., On the Calculation of Interlaminar Normal Stress in Composite Laminates, Journal of Composite Materials, 8, (1974), pp. 65–81.
4. Pagano N. J. and Soni S. R., Models for Studying Free-edge Effects, In: Interlaminar Response of Composite Materials, Pagano N. J. (ed.), Elsevier Science Publishers B.V., (1989), pp. 1–68.
5. Wang A. S. D., Slomiana M. and Bucinell R. B., Delamination Crack Growth in Composite Laminates, In: Delamination and Debonding of Materials, Johnson W. S. (ed.), Philadelphia, American Society for Testing and Materials, (1985), pp. 135–167.
6. Crossman F. W. and Wang A. S. D., The Dependence of Transverse Cracking and Delamination on Ply Thickness in Graphite/Epoxy Laminates, In: Damage in Composite Materials, Reifsnider K. L. (ed.), Ann Arbor, American Society for Testing and Materials, (1982), pp. 118–139.
7. O'Brien T. K., Characterisation of Delamination Onset and Growth in a Composite Laminate, In: Damage in Composite Materials, Reifsnider K. L. (ed.), Ann Arbor, American Society for Testing and Materials, (1982), pp. 140–167.
8. Kim R. Y. and Soni S. R., Experimental and Analytical Studies on the Onset of Delamination in Laminated Composites, Journal of Composite Materials, 18, (1984), pp. 70–76.
9. Rots J. G., Computational Modeling of Concrete Fracture, Dissertation, Delft Univ. of Techn., Faculty of Civil Engng., 1988.
10. Schellekens J. C. J., Interface Elements in Finite Element Analysis, Report TU Delft 25.2-90-2-17, TNO-IBBC BI-90-165, 1990.
11. Riks E., An Incremental Approach to the Solution of Snapping and Buckling Problems, Int. J. Solids Structures, 15, (1979), pp. 529–551.
12. De Borst R., Nonlinear Analysis of Frictional Materials, Dissertation, Delft Univ. of Techn., Faculty of Civil Engng., 1986.
13. Wang A. S. D., Fracture Analysis of Interlaminar Cracking, In: Interlaminar Response of Composite Materials, Pagano N. J. (ed.), Elsevier Science Publishers B.V., (1989), pp. 69–109.
14. Hellen T. K., On the Method of Virtual Crack Extensions, Int. J. Numer. Meth. in Engng., 9, (1975), pp. 187–207.
15. Tsai S. W., Composites Design, Dayton, Ohio, 1988, Think Composites.